Smart Grid and Renewable Energy, 2013, 4, 409-418
http://dx.doi.org/10.4236/sgre.2013.45047 Published Online August 2013 (http://www.scirp.org/journal/sgre)

PV-Grid Tie System Energizing Water Pump

Sameer Khader, Abdel-Karim Daud

Electrical Engineering Department, Palestine Polytechnic University (PPU), Hebron, Palestine.
Email: daud@ppu.edu

Received June 27th, 2013; revised July 27th, 2013; accepted August 4th, 2013

ABSTRACT

This paper presents the behaviours of three-phase induction motor driving centrifugal pump under various solar irradiation levels, where the motor speed and torque depend on the source voltage and frequency, while the water-flow rate depends on the motor speed, density, and static head according to affinity flow. Matlab/Simulink model is proposed for studying the behaviours of these machines with respect to water flow capacity, motor current, electro-magnetic torque, and motor efficiency. The proposed photovoltaic with maximum power point tracking model based on observation and perturbation (O&P) maximum power tracking model is applied. The output voltage is regulated throughout Buck-Boost converter with purpose maintaining the output voltage at predetermined values. Since Induction motors are widely used in pump systems, the electromagnetic torque, water-flow rate are studied for various source frequencies. Comparison analysis is conducted for both motors with respect to water flow-rate, heads elevation, and motor current. In addition to that, the proposed system presents Photovoltaic-Grid (PV-Grid) Integrated model, where the power shortage required for normally operation of the pump is drawn from the electrical grid.

Keywords: Photovoltaic; Induction Motor; Centrifugal Pumps; Electrical Grids; Matlab/Simulink

1. Introduction

Photovoltaic energy resources presents alternative and friendly to the environment sources. It presents unique solution for providing remote area with clean and sustainable energy during the daytime in heating, lighting, refrigeration and water pumps systems [1-3] without the need of battery system, while during the night time the accumulated energy can be fully or partially used to cover the energy domain. The output circuit connected to the photovoltaic system is usually dc-dc converters mainly boost choppers in order to boost the voltage to the predetermined levels.

The DC/DC converters are widely used in regulated switch mode power supplies, where the input voltage to these converters varies in wide range especially in the case of Photovoltaic (PV) supply source due to unpredictable and sudden change in the solar irradiation level as well as the cell operating temperature. Several connection topologies concerning the switching systems have been proposed [4-8] aiming at realizing the required voltage level during different periods of day for certain applications such as pumps, motors in general and power supplies.

On the other hand water flow consumption determines the rate of motor speed according to affinity law [6,7] which in turn determines the elevation (static head) and consumed power. Variable Frequency Drive (VFD) can be applied to achieve up mentioned facts.

The proposed model consists of several modules as shown in **Figure 1** with the following functions:

- **PV Photovoltaic Array** (*PV*) that converts the solar irradiation into voltage V_{pv} and current I_{pv}.
- **Buck-Boost DC Chopper** Module that boosts up the PV voltage to the predetermined levels. Conversely in case of high V_{pv} the output voltage is reduced.
- **MPPT**, maximum power point tracking unit that tracks the optimized operation point for power extraction by controlling the chopper duty cycle.
- **Variable Frequency Drive** that controls the speed and torque of three-phase induction motor driving centrifugal pump by controlling the voltage and frequency.
- **Speed-Flow Control Unit** that determines the required voltage and frequency aiming at regulating the motor speed and torque according to actual water flow consumption.

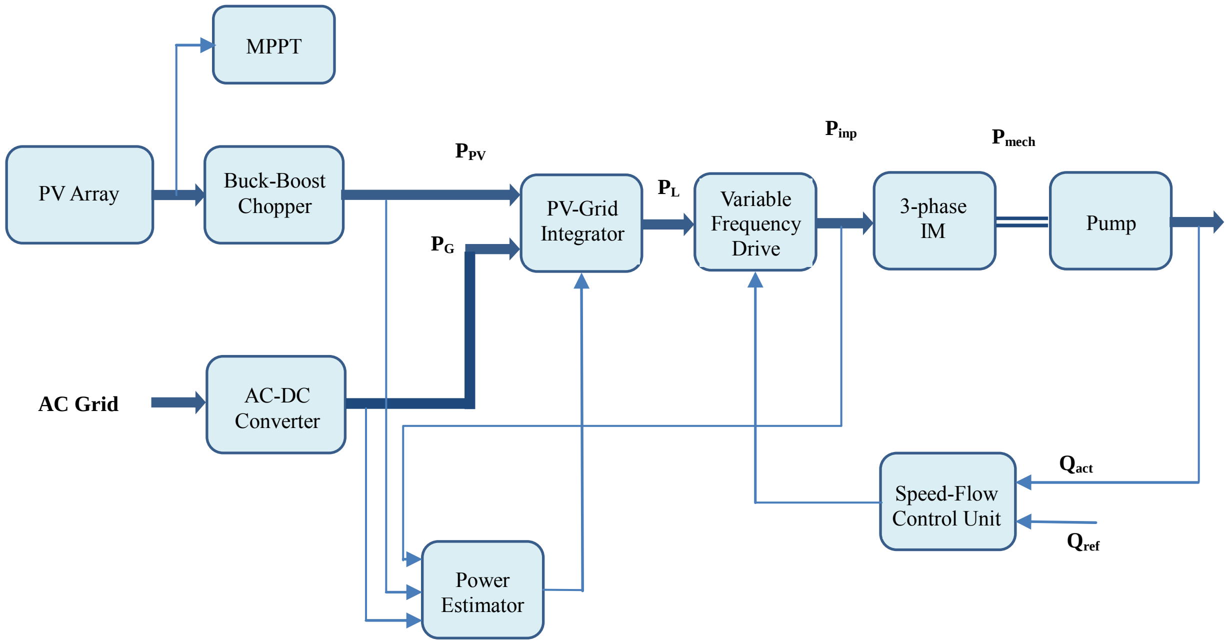

Figure 1. Functional block diagram of proposed model.

- **Power Estimator** that detects the available P_{pv} power, the consumed motor power P_L and the amount of power shortage P_G that should be supplied from AC-grid.
- **PV-Grid Integrator** that provides the load with necessary power taken from either one of the sources *PV* or AC grid, or from both.
- Amount of power shortage P_G that should be supplied from AC-grid.
- **AC-DC Converter** that converts the grid voltage into smoothed DC voltage that should be easily tied to the PV output terminal aiming at avoiding synchronizing procedures.

The proposed model differs from other models, where the system is consumed energy from the grid in case of energy shortages and night time operation. It is fully simulated using Matlab/Simulink, where the system parameters can be changed and investigated.

2. Modeling of Proposed Electrical Model

2.1. PV Performances

The application of Photovoltaic solar energy in energizing electrical load on-grid connected, where the pump power is controlled based on the extracted from the PV module power.

2.1.1. Photovoltaic Model Interpretation

Basically, PV cell is a P-N semiconductor junction that directly converts light energy into electricity. It has the equivalent circuit shown in **Figure 2** [9,10].

The following are the simplified equations describing the cell output voltage and current:

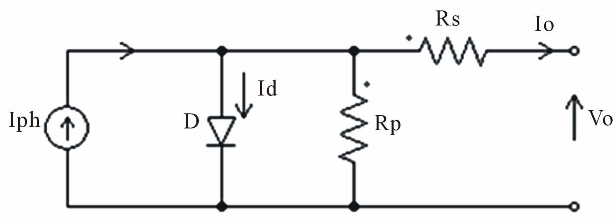

Figure 2. Equivalent circuit for PV cell.

$$V_o = \frac{A\cdot K\cdot T_c}{q}\ln\left(\frac{I_{ph}+I_d-I_o}{I_o}\right)-R_s\cdot I_o \qquad (1)$$

$$I_o = N_p\left(I_{ph}-I_d\left(e^{\frac{q\cdot V_o/N_s}{A\cdot K\cdot T_c}}-1\right)\right) \qquad (2)$$

$$I_d = I_{or}\left(\frac{T_c}{T_r}\right)^3\cdot e^{\frac{q\cdot E_g}{B\cdot K}\left(\frac{1}{T_r}-\frac{1}{T_c}\right)} \qquad (3)$$

$$I_{ph} = N_p\cdot\left\{I_{sc}\cdot\phi_n + I_t\left(T_c-T_r\right)\right\};\ \phi_n = G/G_r \qquad (4)$$

The idealistic diode idealistic factors A & B are with values vary between 1 and 2 depending on I-V performance shaping and approximations.

2.1.2. Photovoltaic I-V Performance

In order to study the I-V performance of the PV circuit and to look for appropriate dc chopper for boosting up the output voltage to predetermined value it is necessary to illustrate the obtained PV voltage and current for boost chopper according to specifications given in **Table 1** at reference irradiation (G_r = 1000 W/m^2). The PV Array voltage can be obtained by multiplying the module voltage and current by N_{sm} and N_{pm}. **Figure 3** illustrates the proposed PV array built in Matlab/Simulink [11] with R-L load, where the obtained results for different variation levels are presented. From these performances it is shown that the total output PV voltage and current varies according to irradiation level with approximated 65 W maximum power at G = 1000 W/m^2.

Table 1. Data specification for PV Array.

q	K	I_{ph}	I_d	R_S	R_P
1.602e - 19 C	1.38e - 23J/°K	4 A	0.2 mA	1 mΩ	10 kΩ
N_S	N_P	V_O	V_{OC}	I_{SC}	V_{MPP}
38	4	0.6 V	21.5 V	4 A	17.5 V
I_{MPP}	N_{Sm}	N_{Pm}	V_{pv}	R_{load}	T_C
3.7 A	6	1	130 V	44 Ω	25°C

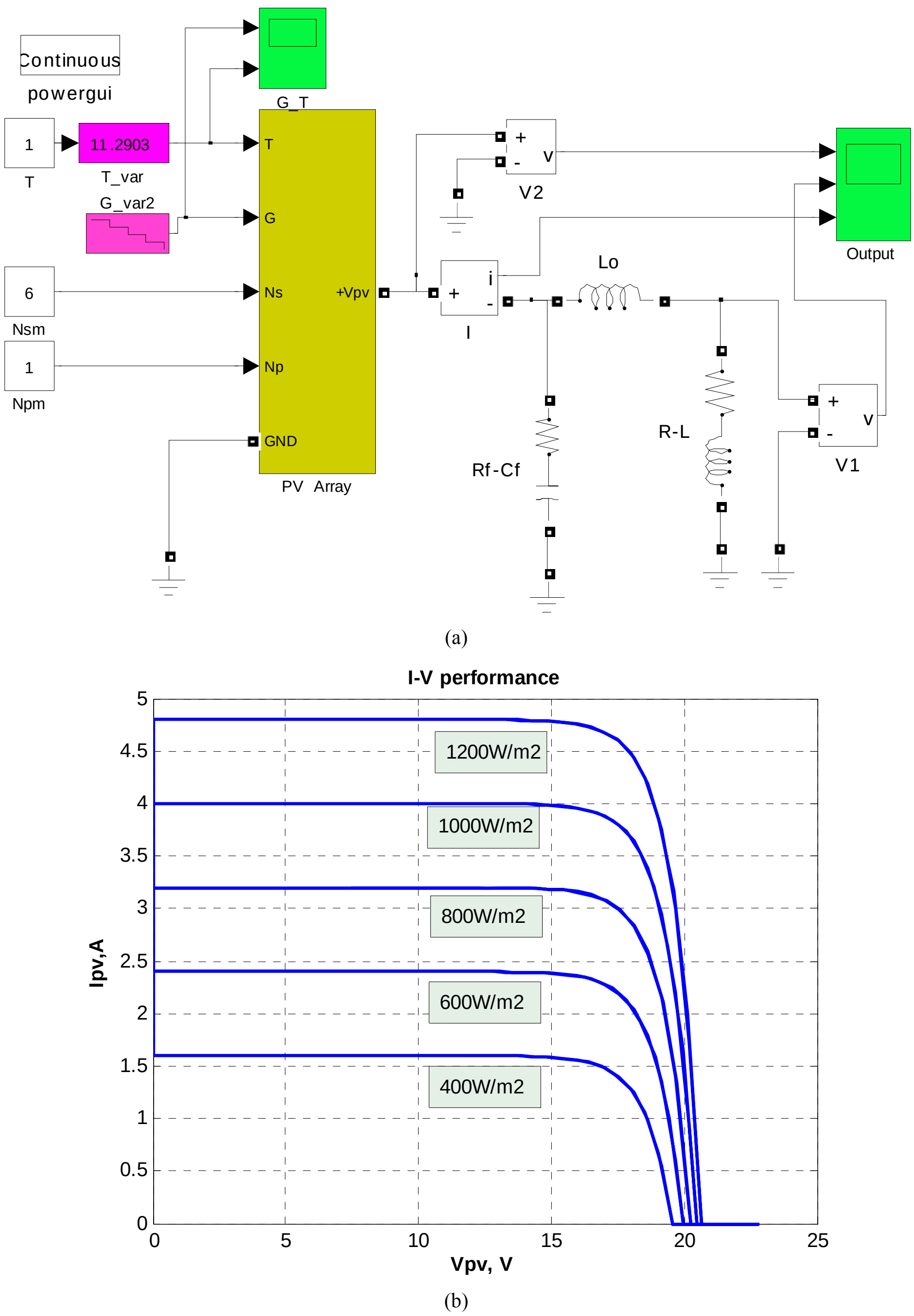

Figure 3. PV model with I-V performances. (a) Proposed model for PV array in Simulink environment; (b) I-V performance of PV module.

2.2. The Integration of PV with Water Pumping System

A centrifugal pumps are used as electrical load [6], where the pump power, speed and torque are directly affected by either load-side parameters in form of water flow-rate, static head, water pressure, and line side in form of solar irradiation, weather conditions, and extracted power. **Figure 4** illustrates PV solar system energized water pump installation, where the water pumping system can be directly energized from the PV or indirectly throughout battery bank [10]. Both configurations have their advantages and disadvantages.

Direct-coupled pumping systems illustrated in **Figure 4(a)** are sized to store extra water on sunny days so it is available on cloudy days and at night. Water can be stored in a larger-than-needed watering tank or in a separate storage tank and then gravity-fed to smaller watering tanks. Water-storage capacity is important in this pumping system.

While **Figure 4(b)** illustrates battery-coupled water pumping systems which consist of photovoltaic (PV) panels, charge control regulator, batteries, pump controller, pressure switch, tank, and AC water pump. The electric current produced by PV panels during daylight hours charges the batteries, and the batteries in turn supply power to the pump anytime water is needed. The use of batteries spreads the pumping over a longer period of time by providing a variable voltage and frequency depending on the water-consumption rate, which in turn reduces the pump losses and increases the battery discharging time which is an important factor during the night and low light periods, the system can still deliver a needed rate of water for livestock.

2.2.1. Centrifugal Pump Performances

According to [8] the power demand of the water pump is expressed using the following expression:

$$P_p = \frac{\rho \cdot g \cdot Q \cdot H}{\eta_p} \tag{5}$$

The pump operational performance which presents the relationships between total head including static head and friction head, water flow-rate, and pump efficiency are illustrated in **Figure 5** for certain commercial pump.

By applying the principle of motor-pump power balance, Equation (5) can be integrated with motor speed-torque performance as:

$$\rho \cdot g \cdot Q \cdot H = \eta_p \cdot T_m \cdot \omega \tag{6}$$

Now referring to **Figure 5** where the pump (H-Q) curve is illustrated, which normally used to locate the pump's operation point. For exact determining the mentioned operation point there is a need to determine the total head of the installation H_A, which is the sum of the

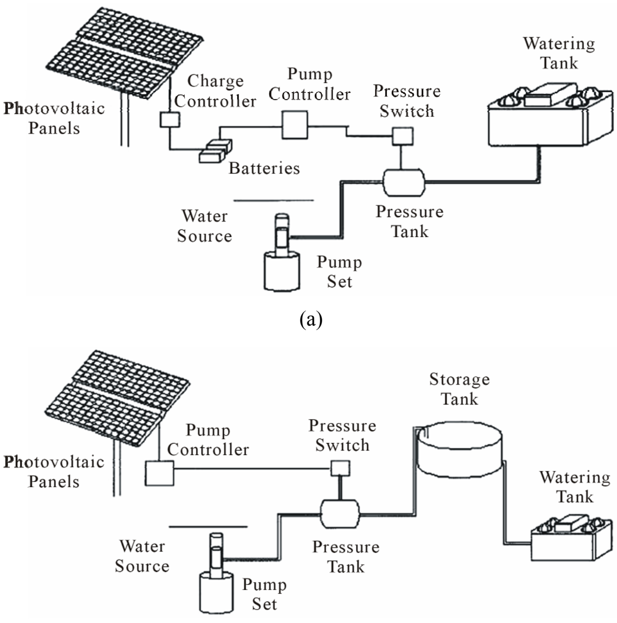

Figure 4. PV system energizing water-pumping systems. (a) Direct-coupled water-pumping systems; (b) Battery-coupled water-pumping systems.

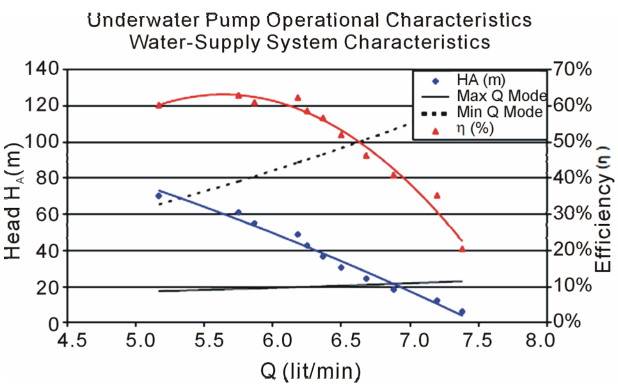

Figure 5. Water pump operational characteristic.

static head H_S known as elevation difference, and the network hydraulic losses H_L, thus :

$$H_A = H_s + H_L = h + \xi \cdot Q^2 \tag{7}$$

The friction coefficient ξ depends on the system installation, pipes section, and liquid viscosity. The operation point results by the application of the following equation:

$$H = H_A \tag{8}$$

This condition can be obtained by intersecting of the corresponding curves of **Figure 5**.

2.2.2. Electrical Motor Performances

Centrifugal pumps can be driven by either direct current motors [9] or alternating current motors, mainly induction motors [12]. Due to massive exploitation of induction motors in water pump system, the electromagnetic performances of induction motor are going to be described in the following sections.

2.2.2.1. Mathematical Model

Utilizing the induction motor as prime mover source for providing the pump machine with needed energy. Three-phase induction motor is going to be describes as follows [13].

The stator winding is supplied with balanced three-phase ac voltages, which produces induced voltages in the rotor windings due to transformer action. The distribution of stator windings is arranged, so that there is an effect of multiple poles, producing several cycles of magneto motive force (or field) around the air gap. This field establishes a spatial distribution sinusoidal flux density in the air gap. The synchronous speed of the rotating filed is defined by [14]:

$$\omega_{sn} = 4\pi f_n / p \quad \text{and} \quad n_{sn} = 120 \cdot f_n / p \tag{9}$$

A very useful quantity in studying induction machines is the slip s:

$$s = \frac{\omega_s - \omega}{\omega} = \frac{n_s - n}{n} \tag{10}$$

Per-phase equivalent circuit of a three-phase induction motor is shown in **Figure 6(a)** [15]. An expression for the torque of an induction machine as a function of its slip may be obtained by application of Thevenin's theorem to the circuit model to the circuit model (**Figure 6(b)**). The rotor circuit, as referred to the stator, may be considered as being attached to an equivalent Thevenin generator, as shown in **Figure 6(b)**.

As well known for electrical machines theory in order to maintain constant maximum torque and to avoid motor saturation and to minimize the losses the (volt/hertz) ration must be kept constant for speeds less than the synchronous speed, while for speeds over the synchronous the voltage is maintained at its rated value and the frequency is increased over the rated limits.

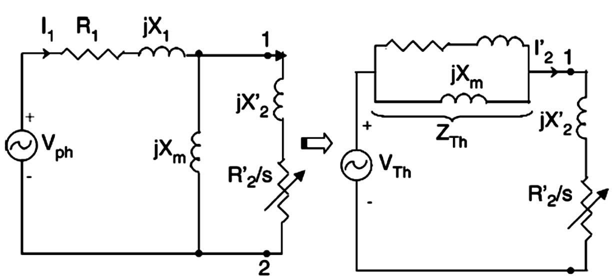

(a) (b)

Figure 6. Equivalent circuit of 3-phase induction motor. (a) Equivalent circuit for one phase; (b) Application of Thevenin's theorem.

According to [13] if the frequency is increased above rated value, the flux and torque would decrease. If the synchronous speed corresponding to the rated frequency f_n is called base speed $\omega_{sn,}$ or n_{sn}, the synchronous speed at any other frequency becomes:

$$\omega_s = K_o \cdot \omega_{sn} \text{ or } n_s = K_o \cdot n_{sn} \tag{11}$$

where $K_o = f / f_n$.

Substituting Equation (11) in Equation (17) the electromagnetic torque can be expressed as:

$$T_{em} = 2 \cdot k_p \frac{K_v^2}{\left(\frac{R_1}{f}\right)^2 + \left(\frac{X_1 + X_m}{f_n}\right)^2} \cdot \frac{R'^2 / s \cdot f}{\left(\frac{s \cdot R'_{th} + R'^2}{s \cdot f}\right)^2 + \left(\frac{X'^{th}}{f} + \frac{X'^2}{f_n}\right)^2} \tag{12}$$

where $K_p = X_m^2 / 2w_{sn}$.

According to [15] $K_v = V_{Ln} / f$ for $f > f_n$; and $K_v = f\left(T_{\max}, R_1, X_1, f, X_{th}, R_{th}, \cdots\right)$ for $f < f_n$.

The electromagnetic power P_{em} and the losses can be defined as follow:

$$P_{em} = \omega \cdot T_{em} = K_o \cdot \omega_{sn}\left(1 - s\right) T_{em} = P_{mech} + P_{const} \tag{13}$$

Varying the frequency of the motor causes significant change in the drawn by the motor current, and in turn the consumed power. According to **Figure 6**, the power and current can be given as follows:

$$\begin{aligned} I_{L1} &= \frac{V_{ph}}{\left|Z_{in}\right|};\ P_{inp} = \sqrt{3} V_{LL} \cdot I_{L1} \cdot \cos\phi;\ \phi = \tan^{-1}\left(\frac{X_{inp}}{R_{inp}}\right) \\ Z_{in} &= R_{inp} + jX_{inp} = R_1 + jK_o \cdot X_1 \\ &\quad + jK_o \cdot X_m \left\| \left(R'_2 / s + jKo \cdot X'_2\right)\right. \end{aligned} \tag{14}$$

2.2.2.2. Simulation Results

Considering the rated parameter values of the selected induction motor [15]:

$n = 2835$ rpm; $Pn = 1100$ W; $Vn = 127$ Vac; $R_1 = R'_2 = 1.27\ \Omega$; $X_1 = X'_2 = 3.860\ \Omega$; $Xm = 60\ \Omega$.

Substituting the outlined motor parameters in the developed mathematical model, we obtain through simulation the motor torque as a function of speed (and slip) for different supply frequencies as shown in **Figure 7**. For a constant (V/F) ratio, the motor develops a constant maximum torque, except at low speeds (or frequencies). From this curve the motor develops two operation modes: constant torque modes for frequencies less than the rated where the torque is maintained constant; and constant power mode for frequencies greater than the rated where the speed exceeds the synchronous and the torque falls down keeping the power at constant value.

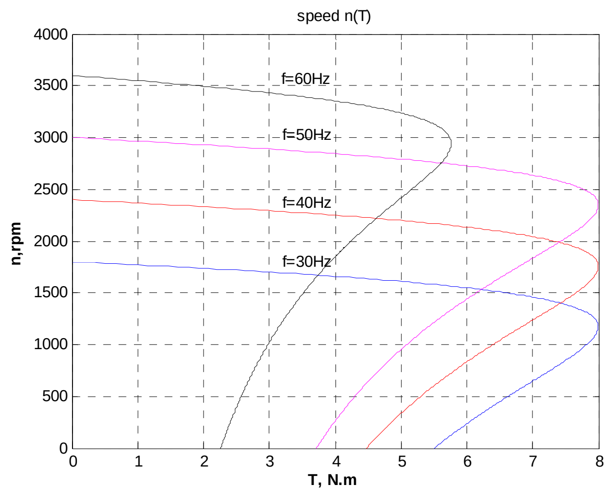

Figure 7. Simulation results of the mechanical performance of three-phase induction motor.

Having the mechanical performance of the motor at various frequencies, where two operation mode can be applied constant torque (V/F = const) & constant power (V = const, $f > f_n$) throughout VFD inverter we can build the pump performance. Way out from the natural curve of the pump at rated motor speed, where f, H & Q are nominal values, and known from the pump data sheet.

Taking into consideration the affinity law and derived equation stated in [16,17] for various motor speeds the water flow-rate changes at various elevations (static head) as follows:

$$\frac{H}{H_n} = \left(\frac{n}{n_n}\right)^2 = \left(\frac{f}{fn}\right)^2; \quad \& \quad \frac{P_{mech}}{P_{mechn}} = \left(\frac{f}{fn}\right)^3 \tag{15}$$

Applying Equation (15) in presented model requires to select the whether the pump operates at maximum efficiency where the water-flow rate has optimized value ($Q_{\eta\,max}$), thus:

$$\frac{H}{H_n} = \begin{cases} \left(\dfrac{f}{f_n}\right)^2; \text{ for } Q < Q_{\eta\max} \\ \left[1 \pm \left(\dfrac{Q - Q_{\eta\max}}{Q_{\eta\max}}\right)^2\right] \cdot \left(\dfrac{f}{f_n}\right)^2; \text{ for } Q > Q_{\eta\max} \end{cases} \tag{16}$$

where

$$Q_{\eta\max} = Q_{n\eta\max} \cdot \left(\frac{f}{f_n}\right);$$
$$Q_{n\eta\max} = Q \;\; @ \;\; fn = 50 \text{ Hz} \;\; \& \;\; \eta_{\max} \tag{17}$$
$$\left(+ \, for \; f > f_n \text{ and } - f < f_n\right)$$

The simulated results are displayed in **Figure 8**, where the pump flow-rate and static heads changed at different frequencies. According to pump data sheet the value of ($Q_{\eta\,max}$ = 9.5 m^3/hr) is taken as a reference value obtained at maximum efficiency and 50 Hz frequency. Also it's shown that regulating the source frequency directly affects the static head and water-flow rate.

On other hand regulating the frequency causes significant change in motor current as shown in **Figure 9**, where at low frequency the drawn by the motor current is the highest comparing with others at both operation modes, starting and rated operation.

At different frequencies there is a stable operation points where the motor operates at its rated slip (s_n) where the amount of pumped water depends on the mechanical torque developed at these frequencies and given head. Referring to Equation (6) and substituting the value of rated slip in Equations (12) and (14), the water flow-rate can be written as:

$$Q = \eta_p \frac{4\pi f\left(1 - s_n\right)}{\rho \cdot g \cdot H \cdot P} \cdot T_{em}\left(s = s_n\right) \tag{18}$$

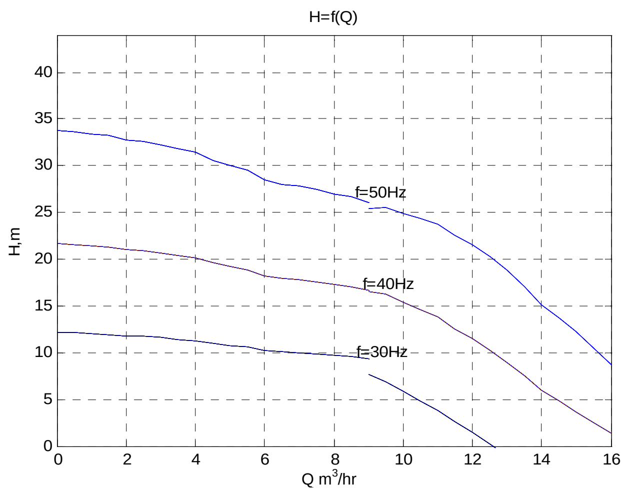

Figure 8. Simulation results of the pump performance H = f(Q).

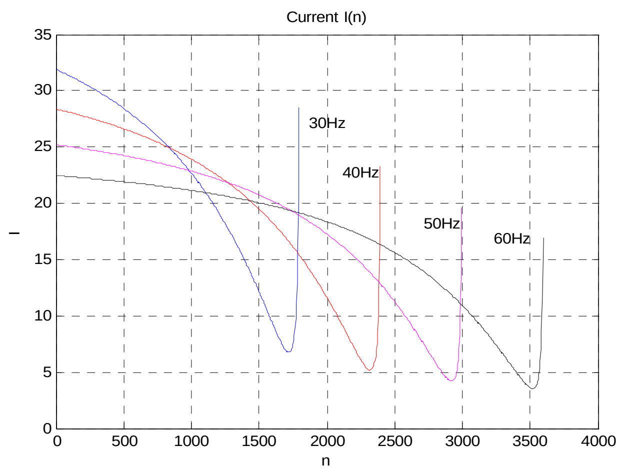

Figure 9. Simulation results of the motor current at various frequencies $I_{ph} = f(n)$.

The obtained simulation results at rated motor operation for various frequencies and elevation are givenin **Figure 10** for water flow-rates at three heads (10 m, 25 m and 40 m) where it can be seen that for frequencies below the rated (f < 50 Hz) Q has quadratic relation with speed.

3. SIMULINK Model of Described Pump System

3.1. Simulation Model

A Matlab/Simulink for proposed mathematical model is presented for induction motor pump, taking into account that varying the motor voltage and frequency in accordance with water flow-rate level saves energy and operates the motor at maximum pump efficiency.

Figure 11 presents the whole Simulink model including solar PVmodel, Variable voltage-variable frequency inverter system, Pump system, and water flow-rate system, that predicts the water flow-rate and regulates both voltage and frequency by using the variable voltage-variable frequency (VFD) technology in order to keep the motor operating at constant torque.

3.2. Simulation Results

The obtained simulation results from above mentioned model are displayed in **Figure 12** for various water flow-rate and corresponding reference and actual speed, where it's shown that the motor adjusts its speed in accordance with the needed flow-rate, which in turn significantly reduces the power consumption.

While **Figure 13** illustrates the generated by PV generator effective power at various radiations and consumed by the pump effective power at water elevation of

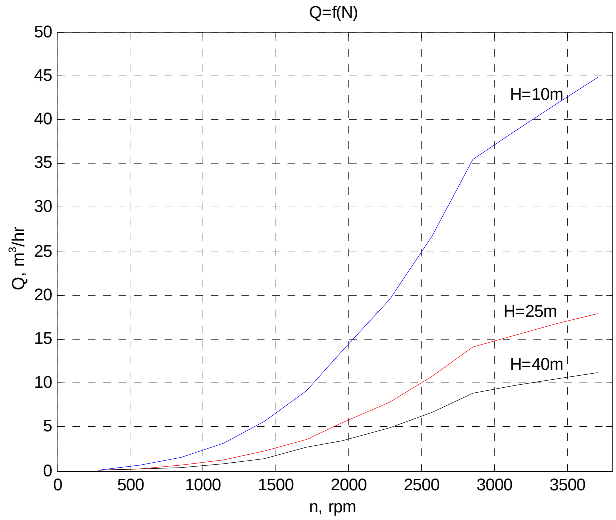

Figure 10. Simulation results for pump performance at different heads (elevations).

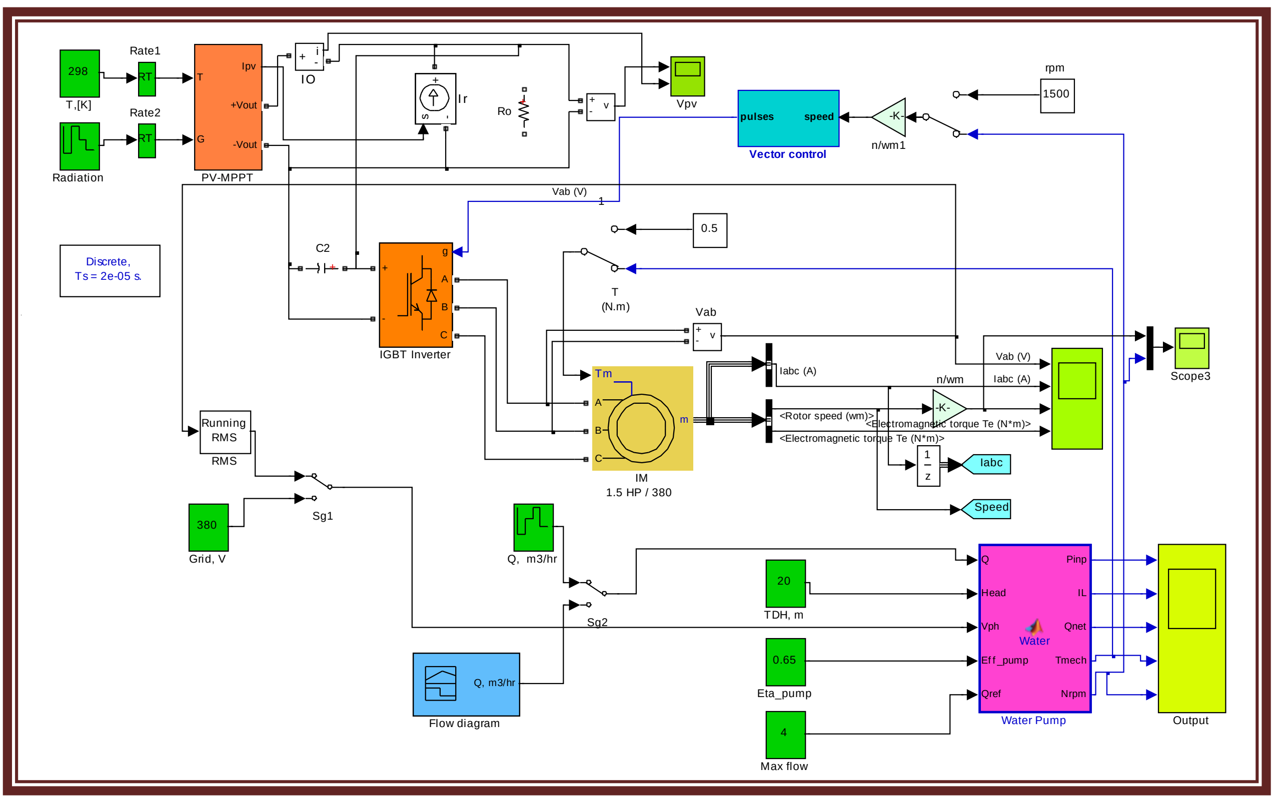

Figure 11. Matlab/Simulink model of induction-motor pump.

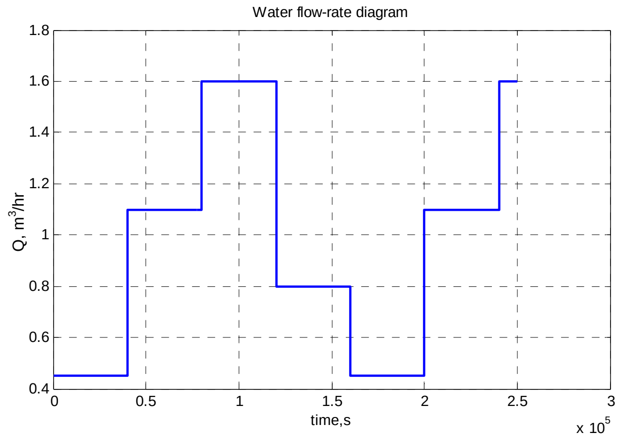

(a)

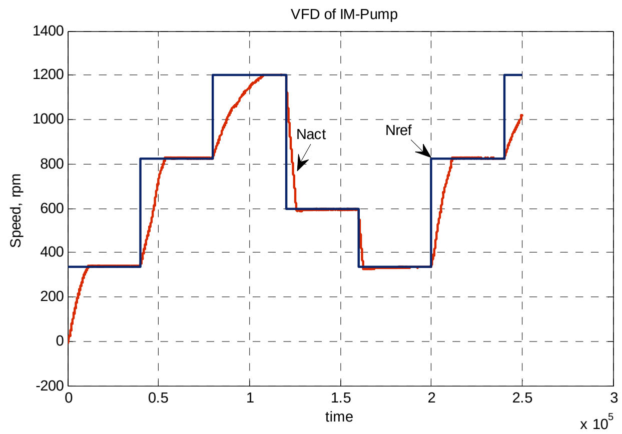

(b)

Figure 12. Simulation results of water flow-rate and obtained speed. (a) Water flow-rate diagram; (b) Pump actual & reference speed at 20 m elevation.

20 m. It can be seen that at various water consumption the PV system is capable to energize the pump system and the excess of power at light consumption rate can be used for energizing another loads. Furthermore applying (VFD) saves energy and gives the pump system the ability for normally operation even at light irradiations or cloudy weather.

3.3. Grid-Integrated Simulation Model

The proposed pump system is mainly energized from the PV source, while the AC utility serves to recover the energy shortages [17]. **Figure 14** illustrates the complete simulation model including power estimator module, grid compensation module, grid-tie module, etc.

Avoiding synchronizing procedure when two AC sources are parallel connected, the AC utility is converted into DC and connected to the load based on switching commands sent by power estimator module to switch Q_4 by mean of the logic depicted in Equation (19).

The total power in form of voltage and current are

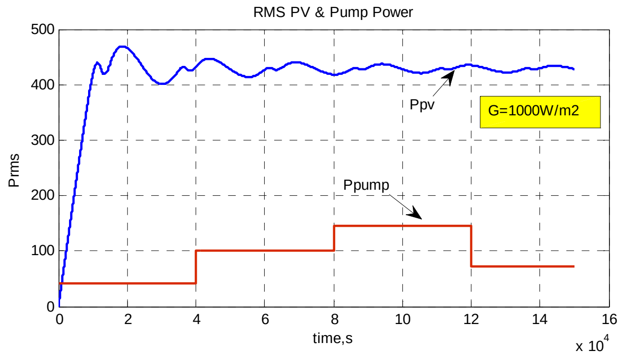

(a)

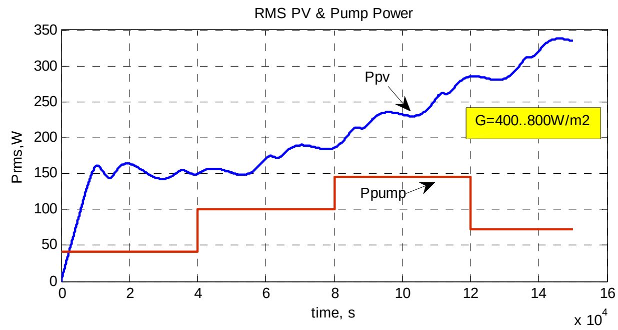

(b)

Figure 13. Generated and consumed power at various irradiations. (a) Power diagram at constant irradiation; (b) Power diagram at various irradiations.

converted into AC through out inverter circuit.

$$Q_4 = \begin{cases} OFF \text{ if } P_{pv} \geq P_L \cdots \text{Pure } PV \text{ Source} \\ ON/OFF \text{ if } P_{pv} \langle\ \rangle P_L \cdots \text{Combined} \\ ON \text{ for Night time.} \end{cases} \quad (19)$$

Figure 15 illustrates the results obtained from the mentioned simulation model, and proposed logic in Equation (19) where it's shown that the grid will be switched on only when there are a power shortages ($P_{pv} < P_{Load}$) and the load needs to be fully energized. Meanwhile, on-off grid connection can be realized in cases of load level fluctuation or cloudy weather. During the night time the load is energized from the AC utility. The proposed circuit can be applied for either AC load or pump system, single or three phase pumps.

4. Conclusions

A complete mathematical model has been developed for studying the pump behaviours at various elevations, water consumption rate and source voltage frequencies.

The proposed PV model consists of variable tracking module and voltage drop compensating module that can be used for either dc or ac loads with precise voltage tracking procedure.

The proposed Simulink model for induction motor

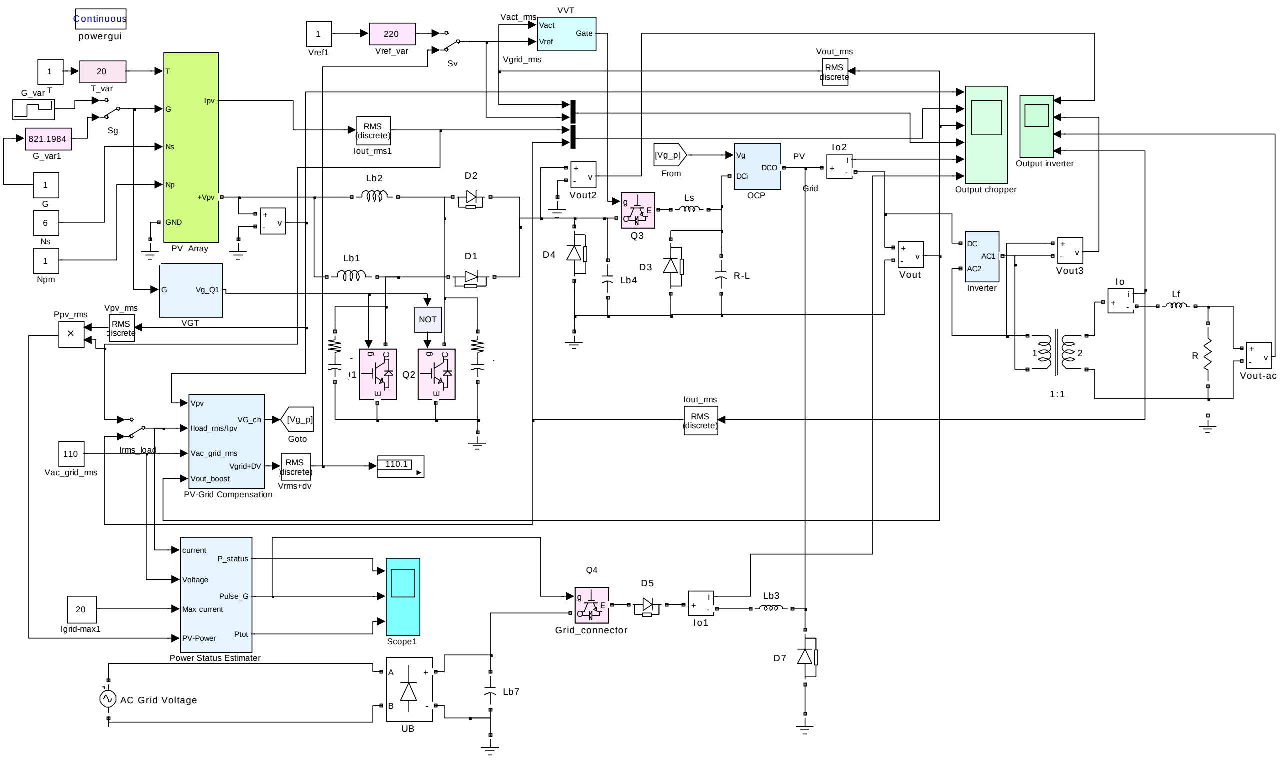

Figure 14. Matlab/Simulink for grid-integrated configuration.

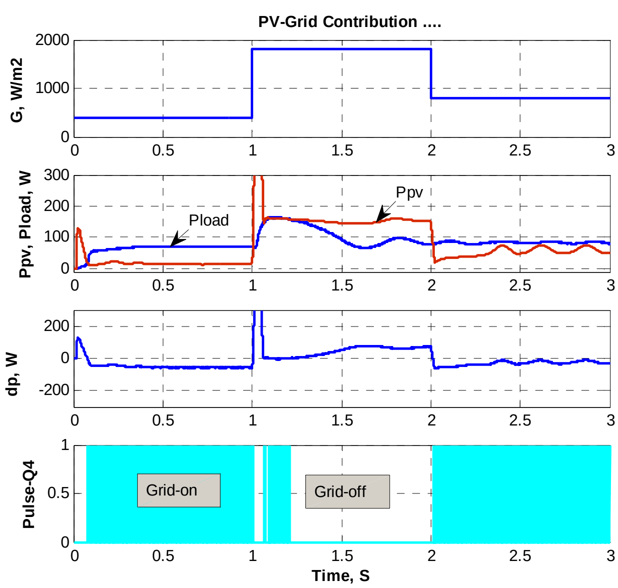

Figure 15. Power diagram at various irradiations & loading status.

pumps shows the effect of applying VFD control on the speed and water-flow rate. The added power-status estimator module creates new aspect to this model, where the power shortages can be measured and delivered from alternative sources or main ac-grid.

The saved energy due to applying VFD control may reaches 30% of consumed power, therefore being more suitable to be energized from PV generator.

REFERENCES

[1] Q. Meng and W. Hu, "Roof Cooling Effect with Humid Porous Medium," *Energy and Buildings*, Vol. 37, No. 1, 2005, pp. 1-9. doi:10.1016/j.enbuild.2003.11.004

[2] P. C. Agrawal, "A Review of Passive Systems for Natural Heating and Cooling of Buildings," *Solar and Wind Technology*, Vol. 6, No. 5, 1989, pp. 557-567. doi:10.1016/0741-983X(89)90091-X

[3] M. Chikh, A. Mahrane and A. Chikouche, "A Proposal for Simulation and Performance Evaluation of Stand-Alone PV Systems," *Proceedings of the 23rd EPVSEC, Valence*, Spain, 2008, pp. 3579-3584.

[4] E. Worrell, S. Ramesohl and G. Boyd, "Advances in EnErgy Forecasting Models Based on Engineering Economics," *Annual Review of Environmental Resources*, Vol. 29, 2004, pp. 345-381. doi:10.1146/annurev.energy.29.062403.102042

[5] S. B. Kjaer, J. K. Pedersen and F. Blaabjerg, "A Review of Single-Phase Grid-Connected Inverters for Photovoltaic Modules," *IEEE Transactions on Industry Applications*, Vol. 41, No. 5, 2005, pp. 1292-1306. doi:10.1109/TIA.2005.853371

[6] I. Odeh, Y. G. Yohanis and B. Norton, "Economic ViabilIty of Photovoltaic Water Pumping Systems," *Journal of Solar Energy*, Vol. 80, No. 7, 2006, pp. 850-860. doi:10.1016/j.solener.2005.05.008

[7] I. I. Lonel, "Pumps and Pumping," Elsevier Publications,

Amsterdam, 1986.

[8] E. V. Meidanis, G. A. Vokas and J. K. Kaldellis, "Theoretical Simulation and Experimental Analysis of a PV-Based Water Pumping System," Lab of Soft Energy Applications & Environmental Protection, TEI of Piraeus. powerelectronics.teipir.gr/Papers/MEDPOWER08_170.pdf

[9] J. Appelbaum and J. Bany, "Performance Analysis of DC Motor Photovoltaic Converter System," *Solar Energy*, Vol. 22, No. 5, 1979, pp. 439-445. doi:10.1016/0038-092X(79)90173-7

[10] M. Abu-Aligh, "Design of Photovoltaic Water Pumping System and Compare It with Diesel Powered Pump," *JJMIE*, Vol. 5, No. 3, 2011, pp. 273-280.

[11] The Mathworks, Inc., "Matlab and Simulink," Version R2010a. http://www.mathworks.com

[12] S. B. Kjaer, J. K. Pedersen and F. Blaabjerg, "A Review of Single-Phase Grid-Connected Inverters for Photovoltaic Modules," *IEEE Transactions on Industry Applications*, Vol. 41, No. 5, 2005, pp. 1292-1306. doi:10.1109/TIA.2005.853371

[13] S. J. Chapman, "Electric Machinery Fundamentals," McGraw-Hill, New York, 2003.

[14] G. McPherson and R. D. Laramore, "An Introduction to Electric Machines and Transformers," Wiley, New York, 1990.

[15] A. K. Daud and M. M. Marwan, "Solar Powered Induction-Motor Water Pump Operating on a Desert Well, Simulation & Field Tests," *Renewable Energy Journal*, Vol. 30, No. 5, 2005, pp. 701-714. doi:10.1016/j.renene.2004.02.016

[16] M. Benghanem and A. H. Arab, "Photovoltaic Water Pumping Systems for Algeria," *Desalination*, Vol. 209, No. 1-3, 2007, pp. 50-57.

[17] S. Khader and A. K. Daud, "Photovoltaic-Grid Integrated System," 2012 *First International Conference on Renewable Energies and Vehicular Technology*, Hammamet, 26-28 March 2012, pp. 60-65. doi:10.1109/REVET.2012.6195249

Nomenclature

A,B	diode idealistic factors
E_g	band gap energy of the semiconductor
f_n	rated supply voltage frequency
g	gravity acceleration (9.8 m/s^2)
G	solar irradiation
G_r	reference solar irradiation
h	reservoir elevation (m)
H	total head (m)
H_A	total installation head (m)
H_S	static head (m)
H_L	network hydraulic losses (m)
ρ	water density (1000 kg/m^3)
η_p	pump efficiency (%)
I_d	diode saturation current
I_{MPP}	PV module current at maximum power
I_o	cell current
I_{ph}	cell photo current
I_{pv}	Photovoltaic current
I_{sc}	short circuit current
I_{or},I_t	constants given at standard conditions
I_{L1}	motor line current
K	Boltzman constant
n	rotor speed in rpm
n_s	motor synchronous speed in rpm
N_p	number of parallel connected cells
N_{pm}	number of parallel connected PV modules
N_s	number of series connected cells
N_{sm}	number of series connected PV modules
p	number of motor poles
P_G	grid power
P_{const}	constant losses power
P_L	load consumed power
P_{em}	electromagnetic power
P_{mech}	net mechanical power
R_{Load}	load resistance
R_p	PV intersinc shunt resistance
R_s	PV intersinc series resistance
R_1	stator resistance of induction motor
R'_2	rotor resistance motor referred to stator
R'_{th}	Thevinen resistance referred to stator
R_{inp}	total input stator resistance
Q	electric charge (*Coulomb*)
Q	water flow-rate (m^3/hr)
P_{pv}	Photovoltaic generated power
PV	Photovoltaic
P_{inp}	motor input power
T_c	cell temperature in Kelvin
T_{em}	electromagnetic torque (N·m)
T_m	motor net mechanical torque (Nm)
T_r	reference temperature in Kelvin
VFD	Variable Frequency Drive
V_{MPP}	PV module voltage at maximum power
V_O	cell output voltage
V_{OC}	PV module open circuit voltage
V_{ph}	terminal phase voltage
V_{pv}	array photovoltaic voltage
V_{th}	Thevinen voltage
X_m	magnetic reactance
X_1	stator reactance of induction mptor
X'_2	rotor reactance of induction motor referred to stator
X'_{th}	Thevinen reactance referred to stator
X_{inp}	total input stator reactance
Z_{th}	Thevinen impedance
Z_{inp}	total input stator impedance
Φ_n	normalized insulation
ϕ	motor phase shift angle
ω	rotor speed in rad/s
ξ	friction coefficient